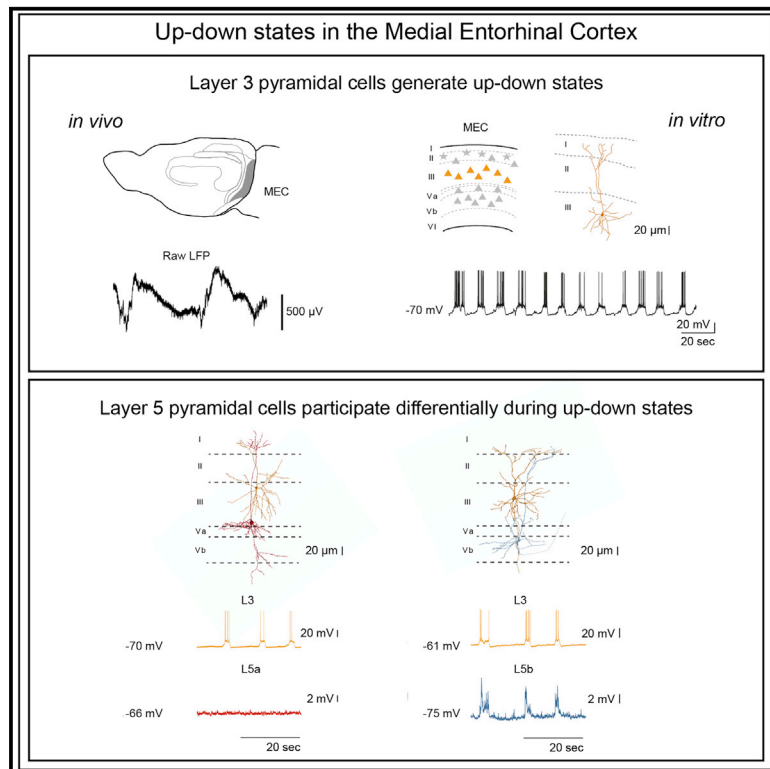


Cell Reports

Layer 3 Pyramidal Cells in the Medial Entorhinal Cortex Orchestrate Up-Down States and Entrain the Deep Layers Differentially

Graphical Abstract



Authors

Prateep Beed, Roberto de Filippo, Constance Holman, ..., Antonio Caputi, Hannah Monyer, Dietmar Schmitz

Correspondence

prateep.beed@charite.de (P.B.),
dietmar.schmitz@charite.de (D.S.)

In Brief

Beed et al. show that layer 3 of the medial entorhinal cortex is necessary and sufficient to generate up-down states locally. This activity propagates differentially to the deeper layers based on the synaptic connectivity between these layers. Layer 5b, which receives hippocampal output, is preferentially activated.

Highlights

- Layer 3 medial entorhinal cortex (L3 MEC) generates up-down states (UDS)
- Inactivation of L3 MEC suppresses UDS
- Two sublayers of L5 MEC differentially participate during UDS
- UDS propagate from L3 to L5b with high fidelity



Report

Layer 3 Pyramidal Cells in the Medial Entorhinal Cortex Orchestrate Up-Down States and Entrain the Deep Layers Differentially

Prateep Beed,^{1,2,9,10,*} Roberto de Filippo,^{1,9} Constance Holman,^{1,9} Friedrich W. Jochenning,^{1,2,7} Christian Leibold,^{3,4} Antonio Caputi,⁵ Hannah Monyer,⁵ and Dietmar Schmitz^{1,2,6,7,8,*}

¹Charité—Universitätsmedizin Berlin, Neuroscience Research Center, 10117 Berlin, Germany

²Berlin Institute of Health, 10178 Berlin, Germany

³Department Biologie II, Ludwig-Maximilians-Universität München, 82152 Munich, Germany

⁴Bernstein Center for Computational Neuroscience Munich, 82152 Munich, Germany

⁵Department of Clinical Neurobiology, Medical Faculty of Heidelberg University and German Cancer Research Center (DKFZ), Im Neuenheimer Feld 280, 69120 Heidelberg, Germany

⁶German Center for Neurodegenerative Diseases (DZNE) Berlin, 10117 Berlin, Germany

⁷Cluster of Excellence NeuroCure, 10117 Berlin, Germany

⁸Einstein Center for Neurosciences Berlin, 10117 Berlin, Germany

⁹These authors contributed equally

¹⁰Lead Contact

*Correspondence: prateep.beed@charite.de (P.B.), dietmar.schmitz@charite.de (D.S.)

<https://doi.org/10.1016/j.celrep.2020.108470>

SUMMARY

Up-down states (UDS) are synchronous cortical events of neuronal activity during non-REM sleep. The medial entorhinal cortex (MEC) exhibits robust UDS during natural sleep and under anesthesia. However, little is known about the generation and propagation of UDS-related activity in the MEC. Here, we dissect the circuitry underlying UDS generation and propagation across layers in the MEC using both *in vivo* and *in vitro* approaches. We provide evidence that layer 3 (L3) MEC is crucial in the generation and maintenance of UDS in the MEC. Furthermore, we find that the two sublayers of the L5 MEC participate differentially during UDS. Our findings show that L5b, which receives hippocampal output, is strongly innervated by UDS activity originating in L3 MEC. Our data suggest that L5b acts as a coincidence detector during information transfer between the hippocampus and the cortex and thereby plays an important role in memory encoding and consolidation.

INTRODUCTION

During non-rapid eye movement (NREM) sleep, many cortical structures display synchronous activity that is characterized by slow-wave oscillatory activity (<1 Hz). Slow-wave oscillatory activity is characterized by alternating between active (depolarized) up states and quiescent (hyperpolarized) down states of neurons, which constitute a sequence of up-down states (UDS). UDS were reported to occur in many species and were detected in several cortical structures (Nir et al., 2011; Steriade et al., 1993; Wilson and Groves, 1981; for a review, see Tukker et al., 2020). It has been shown that UDS can entrain entire cortical columns and propagate between cortical areas as traveling waves (Massimini et al., 2004; Luczak et al., 2007; for a review, see Neske, 2016). The role of UDS is proposed to facilitate information transfer between memory-encoding structures such as the hippocampus and memory consolidation structures in the neocortex (for a review, see Neske, 2016) by influencing synaptic transmission (Bartram et al., 2017) and plasticity (González-Rueda et al., 2018). UDS have been observed during natural sleep (Vyazovskiy et al., 2011) under anesthesia

(Steriade et al., 1993; Wilson and Groves, 1981) and in brain slices (Mann et al., 2009; Sanchez-Vives and McCormick, 2000; Tahvildari et al., 2012). The similarities in the spatiotemporal organization of UDS *in vivo* and *in vitro* enable studies of the underlying circuitry for the generation, propagation, and modulation of UDS at different resolutions by using different techniques.

The entorhinal cortices situated in the temporal lobe are known to be an important relay center for neuronal information between the hippocampus and neocortex. *In vivo* (Hahn et al., 2012; Isomura et al., 2006) and *in vitro* UDS have been described both in the lateral (Namiki et al., 2013) and medial (Mann et al., 2009; Tahvildari et al., 2012) parts of the entorhinal cortices. The medial entorhinal cortex (MEC) is involved in spatial information processing and memory. Recent studies in the MEC addressed questions pertaining to the stability of spatial maps (place and grid cells) during sleep (Gardner et al., 2019; Trettel et al., 2019). Therefore, a better understanding of the local circuit architecture that could maintain and propagate rhythmic activity during different sleep cycles and especially during UDS is gaining importance.



Previous studies provided evidence that UDS activity can be recorded *in vitro* in slice preparations of the MEC. Local field potential and single-cell recordings in superficial layers of the MEC revealed robust slow oscillatory activity indicative of UDS (Mann et al., 2009; Salkoff et al., 2015; Tahvildari et al., 2012). Excitatory and inhibitory neurons in layer 2 (L2) and L3 of the MEC were shown to be active during UDS (Neske et al., 2015; Tahvildari et al., 2012), and inhibition was demonstrated to play an important role in the termination of up states (Craig et al., 2013; Mann et al., 2009).

Although the circuitry that underlies UDS in the MEC has been investigated, questions regarding the generation and propagation of this activity across the laminar architecture of MEC (especially in the deeper layers) remain unanswered. Using *in vivo* recordings, *in vitro* population imaging of calcium activity, and *in vitro* multi-patch recordings, we show in this study that the generation of UDS activity originates in L3 and propagates to L5 of the MEC. Interestingly, L5 pyramidal cells differentially participate during UDS in the MEC—in particular, L5b pyramidal cells, which also receive hippocampal output (Sürmeli et al., 2015), receive UDS-related input from L3 pyramidal cells, whereas L5a pyramidal cells are not recruited. This differential processing of cortical UDS in the deeper layers of the MEC could have wider implications for the circuitry underlying information transfer and memory consolidation between the hippocampus and the cortex (Kitamura et al., 2017; Ohara et al., 2018; Roy et al., 2017).

RESULTS

Up-Down States in the MEC

We recorded stable *in vivo* UDS in the MEC of anesthetized wild-type mice (C57Bl6/n under urethane anesthesia; Figures 1A–1C). Both the frequency (five recordings from five animals; median frequency in the first 5 min \pm interquartile range [IQR] = 0.1500 \pm 0.0117, average frequency = 0.1480 Hz; median frequency in the last 5 min \pm IQR = 0.1500 \pm 0.0558, average frequency = 0.1613 Hz; p = 0.8175, U = 11, Mann-Whitney U test) and up state duration (five recordings from five animals; median duration in first 5 min \pm IQR = 1.855 \pm 0.3187, average duration = 1.51 s, median duration in last 5 min \pm IQR = 1.5338 \pm 0.9538, average duration = 1.756 s; p = 0.4206, U = 8, Mann-Whitney U test) were stable across several minutes of recording (Figure 1D). These measurements are consistent with previously published reports on UDS in the MEC under urethane anesthesia (Isomura et al., 2006; Hahn et al., 2012). Silicon probes were positioned in the superficial layers of the MEC (recording sites mostly in L3; Figure 1B) and slow wave oscillations with nested gamma oscillations were recorded (Figure 1C). We proceeded with an *in vitro* model of UDS in the MEC to investigate in more detail the circuitry that can support the generation and propagation of such slow wave activity.

Since UDS is a population activity, we decided to use mice expressing the genetically encoded calcium indicator GCaMP6f in pyramidal cells in the neocortex by breeding these mice with Nex-Cre mice (Goebbels et al., 2006). This enabled us to image UDS activity at the population level to test for synchronous activation of L3 pyramidal cells in our *in vitro* model (Figure S1). We

imaged the superficial layers of the MEC in five slices from two animals and analyzed between 20 and 33 cells per slice. In sum, we detected 42 synchronous events with coactive cells in a time window of 1 s. In 50% of these events, we observed >10 coactive cells (median of active cells \pm IQR: 11.5 \pm 17; Figures S1A–S1D).

Up-Down States in L3 MEC

It has been shown previously that several cell types, including excitatory and inhibitory neurons in the superficial layers of the MEC, take part in UDS (L1–L3, Mann et al., 2009; Tahvildari et al., 2012). To further differentiate single-cell activity during UDS, we used a multi-patch approach and recorded such slow-wave oscillatory activity simultaneously from two to four cells in the superficial layers of the MEC (Figures 1E and 1F). Based on simultaneously recorded L3 and L2 excitatory cells (L3 = nine cells, L2 = 10 cells; Figures S2A and S2B), we determined that L3 pyramidal cells were the most active cell population. L3 MEC pyramidal cells exhibited a higher spike probability (L3 = 71.26% \pm 11.67%, L2 = 18.41% \pm 9.29%, p = 0.0029, Mann-Whitney U test) and number of spikes per up state (L3 = 5.26 \pm 1.18, L2 = 1.24 \pm 0.50, p = 0.0042, Mann-Whitney U test) compared to those in L2 stellate cells (Figure S2B). Thereafter we focused only on dorsal MEC L3 pyramidal cells and extended our analysis by recording from L3 duplets, triplets, or quadruplets. We quantified the up state duration (1.76 \pm 0.14 s, n = 33 cells; Figure 1H, first panel) and frequency (0.087 \pm 0.008 Hz, n = 33 cells; Figure 1H, second panel) from L3 pyramidal cells and found that our results were congruent with previously reported values (Mann et al., 2009; Tahvildari et al., 2012).

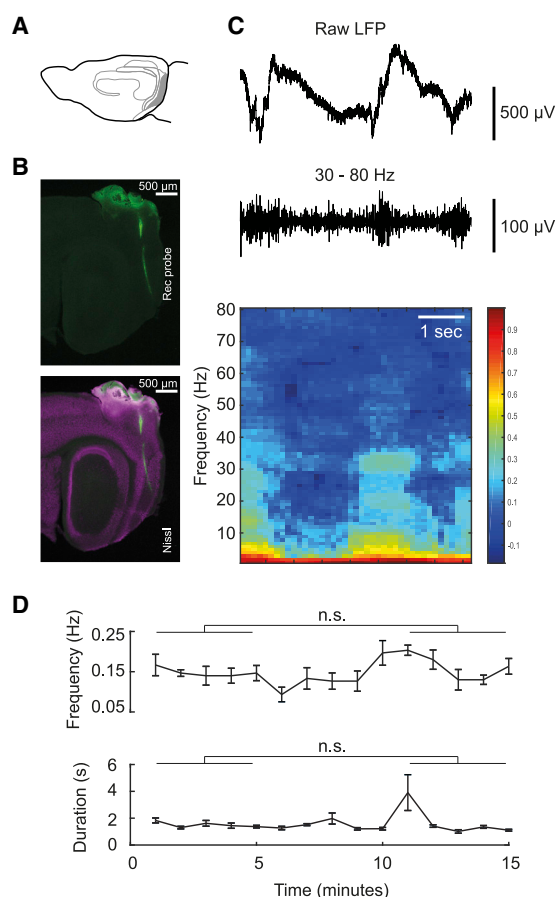
Local MEC Circuitry Can Sustain Up-Down State Activity

Next, we asked whether the MEC alone is endowed with the minimum circuitry necessary to generate and maintain UDS. To this end, we prepared mini-slices of the MEC by making incisions and removing the lateral entorhinal cortex (LEC), hippocampus, and the parahippocampal structures such as the pre- and parasubiculum. L3 pyramidal cells in the mini-slices of the MEC showed robust UDS activity reminiscent of that in intact slices. Up state duration (2.96 \pm 0.12 s, n = seven cells; Figure 1H, third panel) was longer in mini-slices (p = 0.0002, Mann-Whitney U test), and up state frequency (0.109 \pm 0.015 Hz, n = seven cells; Figure 1H, fourth panel) was comparable between mini-slices and intact slices (p = 0.147, Mann-Whitney U test). Hence, we conclude that the isolated MEC, and particularly L3, comprises the circuitry that generates and maintains UDS.

Up-Down States Are Largely Suppressed in the MEC by Silencing L3

Knowing that L3 MEC is the most active layer during UDS, we sought to silence the activity of L3 pyramidal cells to study the impact on UDS in the MEC. We reasoned that silencing L3 pyramidal cells would abolish field UDS activity, if L3 were the generating layer. Alternatively, if other layers in the MEC were responsible and activity propagated to L3, then we would still be able to detect field UDS activity. As a first approach, we uncaged GABA locally on L3 in the MEC during ongoing UDS activity (Figures 2A and 2B). We used a closed-loop photostimulation approach in

MEC *in vivo* up down states



MEC *in vitro* up down states

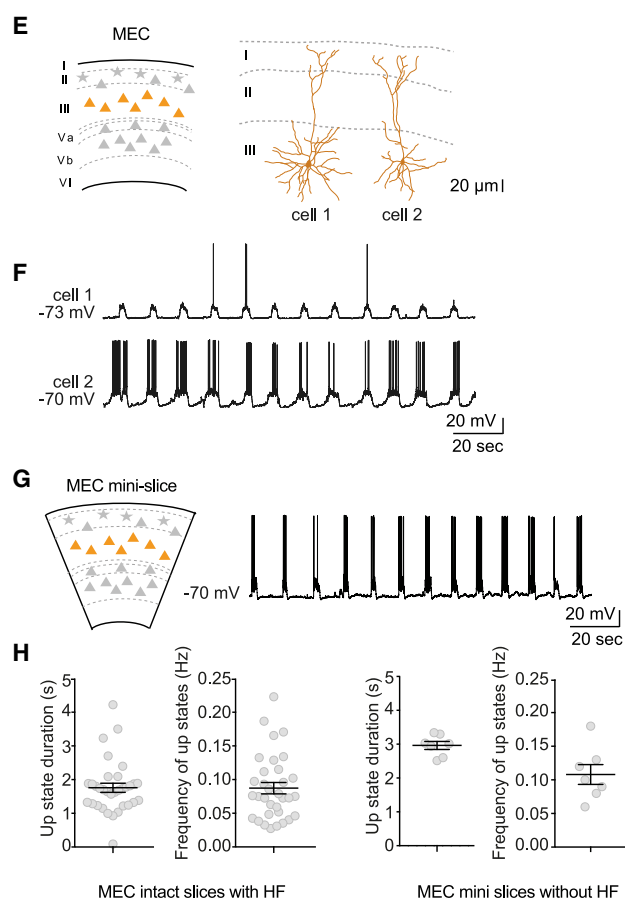


Figure 1. Up-Down States (UDS) in the MEC

(A) Schematic of the sagittal view of the mouse brain, where the MEC is shaded in gray.

(B) Example *in vivo* recordings under urethane anesthesia were targeted to L3 of MEC, as shown by the silicon probe location (top panel in green) and overlay with NeuN staining (lower panel in purple) sagittal section.

(C) UDS from L3 MEC showing slow oscillations (upper panel) with nested gamma frequency oscillations (center panel, band-pass filtered from 30 to 80 Hz). Lower panel shows the spectrogram of the trace above calculated using a Stockwell transform.

(D) Up state frequency and duration remains stable over time under urethane-anesthetized recording conditions ($n =$ five recordings from five animals).

(E) *In vitro* model for UDS in the MEC. L3 is marked in orange. The right panel shows two L3 MEC cells with dense basal dendrites and apical dendrites reaching to the pial surface.

(F) Raw traces showing alternating UDS from the two cells shown in (E) above.

(G) Mini-slices of the MEC were prepared by removing the adjoining hippocampal structures and the presubiculum, parasubiculum, and LEC. The right panel shows a recording from a L3 MEC pyramidal cell demonstrating robust UDS in a reduced mini-slice of the MEC.

(H) Left panel: up state duration and frequency ($n = 33$ cells) in intact slices with hippocampal formation (HF); right panel: in a mini-slice of the MEC ($n =$ seven cells) without HF.

Data are presented as means \pm SEMs. n.s. (non significant) for $p > 0.05$, * $p < 0.05$ and ** $p < 0.01$.

which, as soon as a spike on an up state was detected, blue light was triggered for 500 ms to uncage Rubi-GABA locally. Upon uncaging, we detected an immediate hyperpolarization of the membrane potential to a down state, thereby significantly shortening the up state duration (no uncaging average duration: 3.09 ± 0.07 s, L3 uncaging average duration: 1.79 ± 0.15 s, $p < 0.0001$, Mann-Whitney U test; Figure 2C). Subthreshold events where no spikes were detected were not suppressed, and the average duration of these subthreshold up states during photostimulation trials was not significantly different from baseline (no

uncaging) trials (no uncaging average duration: 2.43 ± 0.21 s, L3 uncaging average duration: 2.63 ± 0.10 s, $p = 0.1427$, Mann-Whitney U test; Figure 2D). The frequency of up states remained unaltered during L3 uncaging and no uncaging trials (no uncaging average frequency: 0.072 ± 0.008 Hz, L3 uncaging average frequency: 0.069 ± 0.018 Hz, $p = 0.9365$, Mann-Whitney U test; Figure 2E). We also analyzed the shortening of up states by defining the duration as the time between the 1st spike on an up state to the termination of that particular up state. The duration was significantly different between L3 uncaging and no

Up state triggered suppression of up states in L3 (*in vitro*)

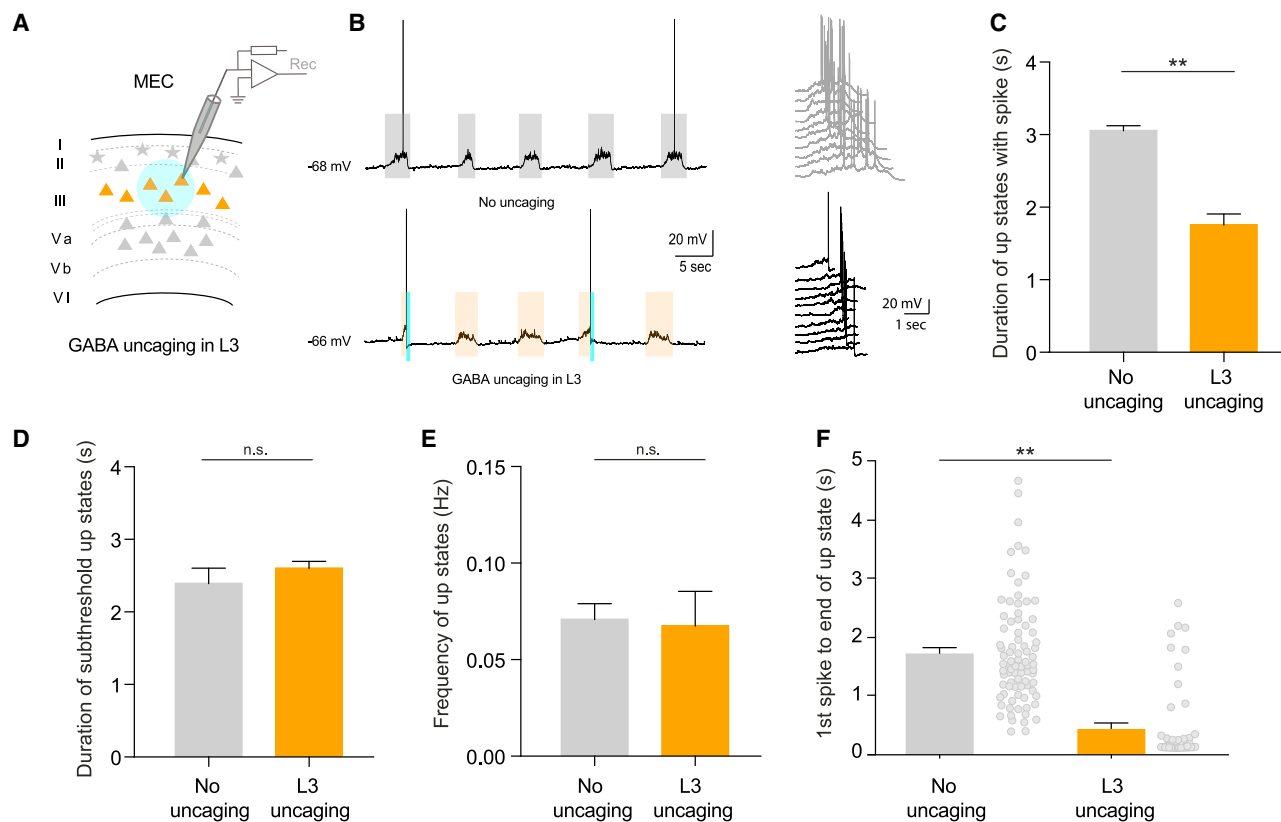


Figure 2. *In Vitro* Spontaneous Up States in the MEC Can Be Suppressed by L3 Hyperpolarization

(A) Schematic of closed-loop GABA uncaging experiments for spontaneously occurring up states. As soon as an up state with spikes was detected, 500 ms of caged GABA was uncaged using blue LED (488 nm) in L3 with no uncaging as control.

(B) Example traces of control (no uncaging) versus GABA uncaging in L3 following a spike on the up state. The shaded gray and orange represent the width of the detected up states. The right panel shows cutout up states in control (above, gray) versus GABA uncaging in L3 (below, black).

(C) Duration of up states with spikes were reduced when GABA was uncaged in L3 compared ($n = 41$ up states from five cells) to no uncaging control ($n = 84$ up states from five cells).

(D) Duration of up states without spikes, which occurred intermittently to those with spikes, was unaltered between the two conditions (no uncaging: $n = 23$ up states from five cells; L3 uncaging: $n = 62$ up states from five cells).

(E) Frequency of up states was unaltered ($n =$ five cells for each condition).

(F) The time from the 1st to the end of up state as a measure of up state silencing shows that GABA uncaging in L3 ($n = 41$ up states from five cells) effectively shortened and suppressed the up state as compared to the no uncaging controls ($n = 84$ up states from five cells).

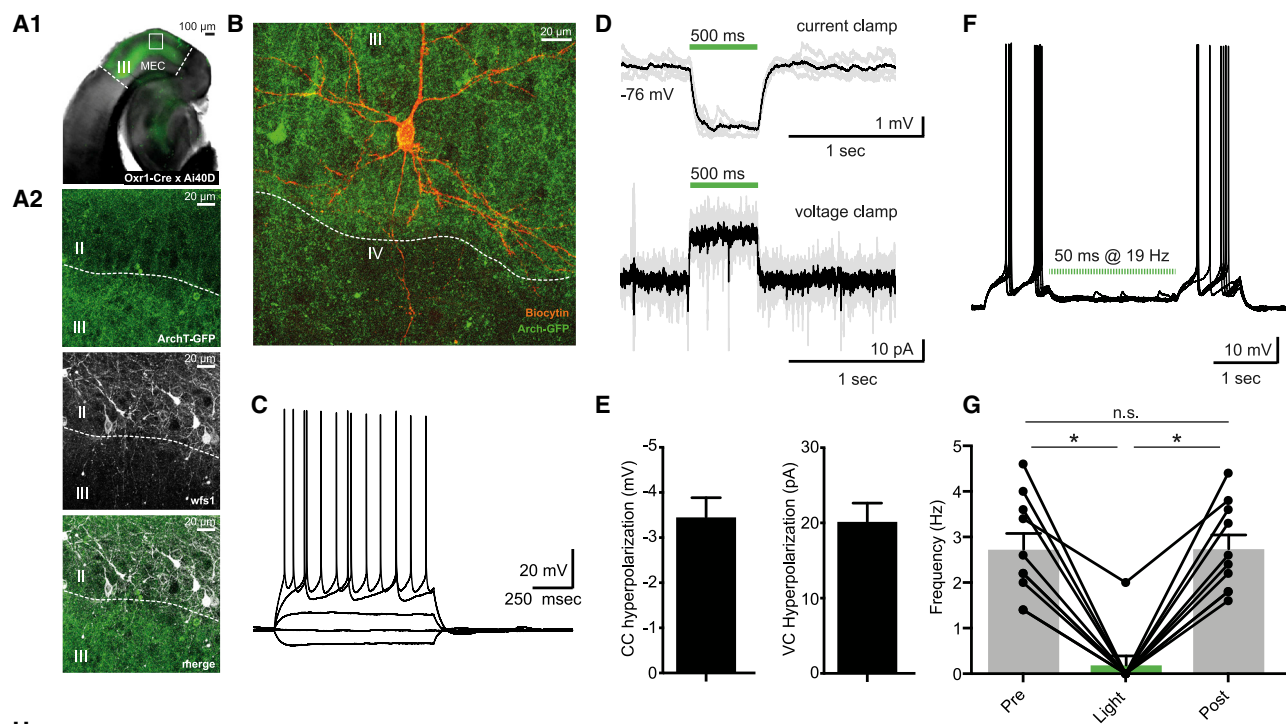
Data are presented as means \pm SEMs. n.s. (non significant) for $p > 0.05$, * $p < 0.05$ and ** $p < 0.01$.

uncaging trials, suggesting that GABA uncaging locally on L3 in the MEC immediately triggered a down state (no uncaging average duration: 1.73 ± 0.10 s, L3 uncaging average duration: 0.43 ± 0.11 s, $p < 0.0001$, Mann-Whitney U test; Figure 2F). Furthermore, hyperpolarizing the deeper layers, namely L5, had no suppressive effect on UDS activity in the MEC. Thus, both spontaneous (Figures S3A–S3C) and evoked (Figures S3D–S3F) up states remained unchanged.

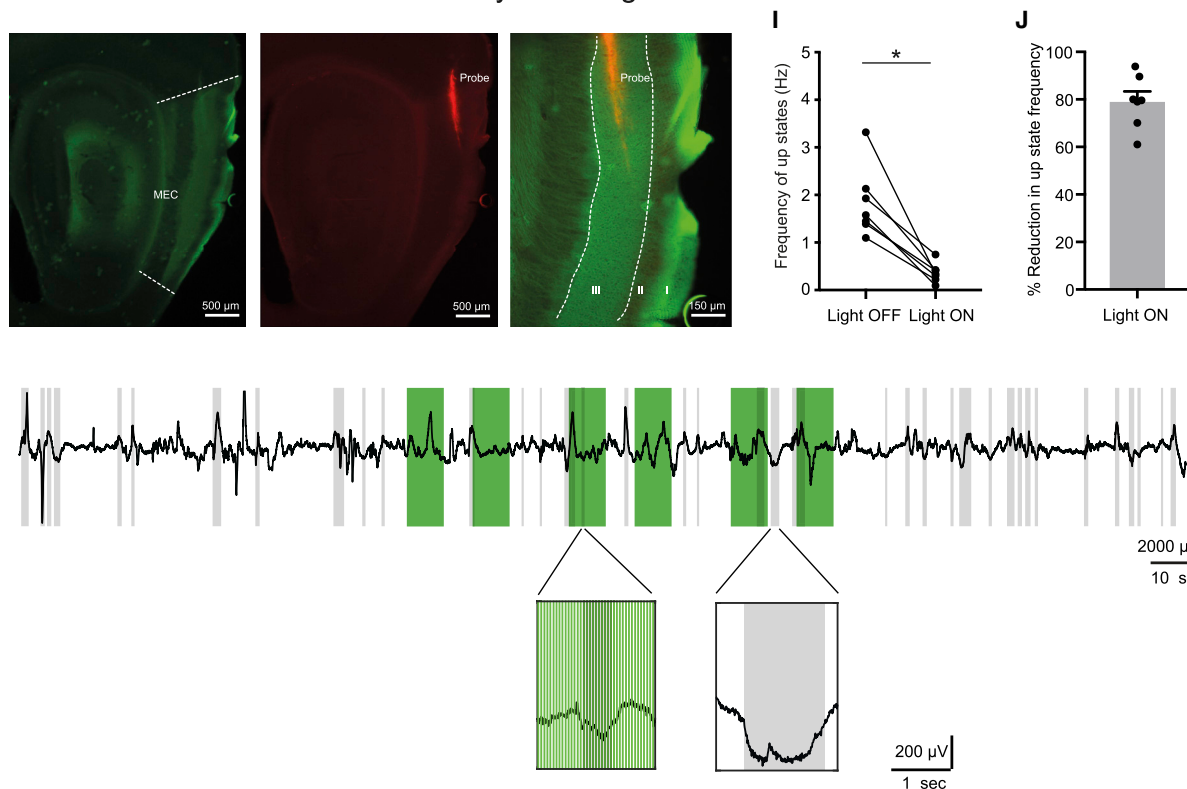
Next, we crossed Oxr1-Cre mice (Suh et al., 2011) with an ArchT (Ai40D) line to express the inhibitory opsin selectively in L3 pyramidal cells in the MEC (Figure 3A1). We verified the spatial selectivity of the expression by co-staining for Wfs1, which marks L2 pyramidal cells (Kitamura et al., 2014). We found

no co-expression of GFP (i.e., Oxr1⁺ putative L3 pyramidal cells) and Wfs1 (i.e., putative L2 pyramidal cells) (Figure 3A2). The GFP expression had a sharp border between L3 and L2, and it was possible to detect terminal branching of the L3 dendrites in L1. As expected, we also saw axonal terminals of L3 MEC pyramidal cells both in the proximal CA1 and distal subiculum, as reported by others for this mouse line (data not shown; Suh et al., 2011). Thereafter, we used *in vitro* slices to quantify the extent of light-induced hyperpolarization L3 pyramidal cells receive (Figures 3B–3E). In current clamp mode, cells were hyperpolarized on average by 3.46 ± 0.43 mV, $n = 18$ cells (Figure 3E) at resting membrane potential, and in voltage clamp (clamped at -60 mV), light-induced hyperpolarization was on average 20.18 ± 2.45 pA,

Oxr1-Cre x Ai40D (ArchT) characterization



H Reduction in in vivo incidence of UDS by silencing L3 MEC



(legend on next page)

$n =$ nine cells (Figure 3E). This prompted the question of whether this hyperpolarization sufficed to suppress spiking in L3 pyramidal cells. Thus, while we injected a 35-pA current for 4 s to evoke spikes, we shone light using a repetitive stimulus of 19 Hz and a pulse width of 50 ms for 2 s (Figure 3F). We were able to completely suppress spiking in 8/9 cells (Figure 3G). In the pre-light period, the frequency of spiking was on average 2.74 ± 0.35 Hz, during light stimulation there was a reduction to 0.2 ± 0.2 Hz, and a subsequent recovery to 2.75 ± 0.31 Hz in the post-light period (2-way ANOVA with multiple comparisons: $p < 0.0001$ for pre versus light, $p < 0.0001$ for light versus post, and $p = 0.99$ for pre versus post).

Inhibition of L3 Pyramidal Cells Suppresses the Frequency of Up States *In Vivo*

Next, we recorded UDS *in vivo* in anesthetized animals as described earlier (Figures 1A–1C) using silicon optrodes. We established a stable baseline of UDS in L3 MEC in Oxr1-Cre x Ai40D mice and then used green light light-emitting diode (LED) (525 nm) to activate archaerhodopsin and silence Oxr1⁺ L3 pyramidal cells directly at the recording site (Figure 3H). The green bars show light ON periods in Figure 3K, and the detected up states are marked with gray-shaded areas. Silencing L3 pyramidal cells caused a large reduction in UDS activity during light ON periods compared to matched light OFF periods (Figures 3I and 3J). During light OFF periods, up states occurred with a median frequency \pm IQR of 1.5791 ± 0.6752 Hz, average = 1.84 Hz. During light ON periods, up states were detected with a median frequency \pm IQR of only 0.3402 ± 0.1780 Hz, average = 0.209 Hz, or an average reduction of 79.1% ($p = 0.016$, $Z = -2.3664$, $n =$ seven recordings from seven animals, Wilcoxon signed rank test). We conclude that L3 MEC pyramidal cells are crucial in generating UDS in the MEC.

Our results using optogenetic inhibition suggest that L3 pyramidal cells are crucial for the generation of UDS in the MEC. However, we wondered whether L3 activity could be controlled in a more time-locked fashion during ongoing UDS activity *in vivo*. Therefore, we used a closed-loop stimulation system that guaranteed the firing of a light pulse each time an up state was detected in anaesthetized mice (see Method Details; Figures S4A–S4C). Here, we found that closed-loop stimulation of L3 pyramidal cells in Oxr1-Cre x Ai40D induced only a subtle, non-sig-

nificant reduction of up state frequency (median baseline frequency \pm IQR = 0.27 ± 0.2458 Hz, average baseline frequency = 0.2693 Hz, median stimulation frequency = 0.14 ± 0.1908 Hz, average stimulation frequency = 0.1700 Hz; $p = 0.1250$, $Z = -1.7529$ Wilcoxon signed rank test, five recordings from five animals; Figure S4D), and the duration of up states was unchanged (median baseline duration \pm IQR = 1.13 ± 1.5701 s, average baseline duration = 1.8784 s, median stimulation duration = 1.32 ± 1.5644 s, average stimulation duration = 2.0101 s, $p = 0.0625$, $Z = -2.0226$, Wilcoxon signed rank test, five recordings from five animals; Figure S4E).

As a control, we repeated the experiment using wild-type mice that were not injected with an optogenetic construct (data not shown). Here, up state-triggered LED activation in L3 led to a trend of increasing upstate frequency (median baseline frequency \pm IQR = 0.14 ± 0.0671 Hz, average baseline frequency = 0.1367 Hz, median stimulation frequency = 0.22 ± 0.1750 Hz, average stimulation frequency = 0.1807 Hz, $p = 0.1875$, $Z = -1.4832$, Wilcoxon signed rank test, five recordings from four animals), while also not interfering with their duration (median baseline duration \pm IQR = 1.46 ± 0.5085 s, average baseline duration = 1.4278 s, median stimulation duration = 1.49 ± 0.5339 s, average stimulation duration = 1.4852 s, $p = 0.3125$, $Z = -1.2136$, Wilcoxon signed rank test, five recordings from four animals; data not shown).

Our *in vitro* experiments indicated that L2 cells were much less active than L3 cells during up states (Figure S2). L2 stellate cells receive strong feedforward projections from L3 pyramidal cells (Winterer et al., 2017), and they selectively target L5b pyramidal cells (Sürmeli et al., 2015). Thus, we took recourse to the Uchl1 mouse line, which allows specific targeting of L2 stellate cells in the MEC (Fuchs et al., 2016), to test whether manipulating L2 neuronal activity interferes with up state dynamics *in vivo*. Using the same optogenetic protocol on Uchl1-Cre mice injected with adeno-associated virus (AAV) conditionally transducing halorhodopsin (Uchl1-Cre x AAV-eNpHR3.0-EGFP; Figures S4F and S4G), we found that, akin to wild-type controls, optogenetic activation of L2 led to a very slight increase in up state frequency (median baseline frequency \pm IQR = 0.25 ± 0.2185 Hz, average = 0.2788 Hz, median stimulation frequency = 0.31 ± 0.1733 Hz, average = 0.3250 Hz, $p = 0.1250$, $Z = -1.8257$, Wilcoxon signed rank test, four recordings from three animals; Figure S4H) and no

Figure 3. L3-Specific Optogenetic Inactivation Suppresses *In Vivo* UDS in MEC

(A1) Oxr1-Cre x Ai40D showing specific expression of ArchT in L3 MEC pyramidal cells. The rectangular box is magnified in A2. (A2) GFP expression is specifically restricted to L3 (top panel, Wfs1 staining delineates the border to L2 (center panel)). The merge shows the specificity of the Oxr1 line to L3 MEC pyramidal cells. (B and C) Biocytin filled L3 pyramidal cell in (B) and characterization of firing pattern in (C). (D) Light-induced hyperpolarization in current and voltage clamp on single L3 pyramidal cells upon activation of ArchT using 550 nm light. (E) Quantification of average light-induced hyperpolarization in current clamp (CC hyperpolarization, $n = 18$ cells) and voltage clamp (VC hyperpolarization, $n =$ nine cells) on L3 pyramidal cells upon activation of ArchT using 550 nm light. (F) Current injection-evoked spikes could be robustly suppressed by activating ArchT on individual L3 pyramidal cells. (G) Reduction of spiking activity in L3 pyramidal cells upon ArchT activation ($n =$ nine cells). (H) Example sagittal section from L3 recording in MEC, showing GFP (left), Dil trace (center), and magnified overlay (right). (I) Frequency of up states during light OFF periods compared to light ON epochs ($n =$ seven recordings from seven animals). (J) Percentage reduction in upstate frequency from values shown in (I). (K) Above: example raw LFP trace from L3 optrode recording. Green-shaded areas indicate light stimulation (light ON periods), and gray-shaded areas show the detected up states. Below: segments of trace magnified to show up states during light ON and light OFF periods. Data are presented as means \pm SEMs. n.s. (non significant) for $p > 0.05$, * $p < 0.05$ and ** $p < 0.01$.

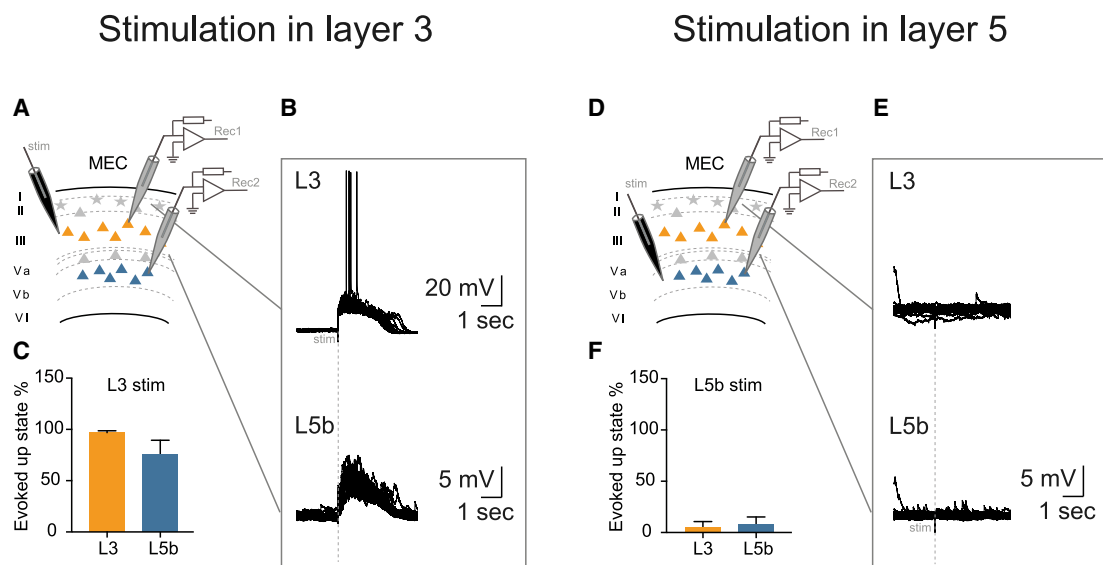


Figure 4. Up States Propagate Unidirectionally from L3 to Deeper Layers

(A) Schematic of the experimental setup. We evoked up states by stimulating in L3 (stim) and recording simultaneously from a L3 (Rec1) and a L5b (Rec2) pyramidal cell.

(B) Parallel recordings from L3 and L5b pyramidal cells while stimulating in L3 evokes reliable up states in both layers.

(C) High probability of evoking up states in L3 and L5b pyramidal cells by stimulating in L3 ($n =$ nine cell pairs each having one L3 and one L5b pyramidal cell).

(D) Stimulation electrode was moved to L5b (stim) while recording from the same duplet (Rec1 and Rec2), as in (A).

(E) Parallel recordings from L3 and L5b pyramidal cells while stimulating in L5b failed to evoke reliable up states in either of the cells ($n =$ nine cell pairs each having one L3 and one L5b pyramidal cell).

(F) Low probability of evoking up states in L3 and L5b pyramidal cells by stimulating in L5b.

Data are presented as means \pm SEMs. n.s. (non significant) for $p > 0.05$, * $p < 0.05$ and ** $p < 0.01$.

change in up state duration (median baseline duration \pm IQR = 1.61 ± 0.9190 s, average = 1.5587 s, median stimulation duration = 1.52 ± 0.6700 s, average = 1.4271 , $p = 0.1441$, $Z = 1.4606$, Wilcoxon signed rank test, four recordings from three animals; Figure S4I).

Taking these data together, a Kruskal-Wallis test demonstrated a near-significant difference in up state frequency across these three mouse lines ($H = 5.643$, $p = 0.0502$; Figure S4J). A Dunn's multiple comparisons test revealed that closed-loop stimulation produced a significant difference in frequency for *Oxr1-Cre x Ai40D* compared to wild-type mice ($p = 0.0467$), while there was no difference between wild-type and *Uchl1-Cre x AAV-eNPHR3.0-EGFP* mice ($p > 0.99$).

Up-Down States Propagate to Deeper Layers Unidirectionally

The deep layers of the MEC include two sublayers of L5 (L5a and L5b) and L6. Recently, L5 MEC has gained renewed attention in regard to pathways and cell types linked to memory consolidation (Ohara et al., 2018; Roy et al., 2017; Sürmeli et al., 2015). We wanted to better understand the propagation of entorhinal inputs during UDS from superficial to deeper layers, particularly in L5b, which also receives hippocampal output. To have a better temporal handle on UDS activity, we evoked up states via a stimulation electrode placed in L3 (evoked up states; Figures 4A and 4B; Mann et al., 2009). We saw robust and reproducible evoked up states in L3 pyramidal cells (9/9 cells). Simultaneously, we re-

corded L5b pyramidal cells, and we detected evoked up states in both L3 and L5b pyramidal cells (8/9 cells exhibited up states) upon stimulation in L3. The probabilities with which up states could be evoked were L3 $97.78\% \pm 0.88\%$ and L5b $77.22\% \pm 12.19\%$ (Figure 4C). However, when we moved the stimulation electrode to L5b, we failed to evoke up states with reliable probability in either L5b or L3 pyramidal cells from the same cell pairs (Figures 4D and 4E). We did observe subthreshold depolarization, which could be classified as a putative up state, in 3/9 L5b pyramidal cells; however, the probability was $<10\%$ on average (L5b = $8.89\% \pm 6.16\%$ and L3 = $6.67\% \pm 3.99\%$; Figure 4F). These results suggest that stimulation-evoked up states in L3 very likely propagate to deeper layers such as L5b. In contrast, up states could not be evoked by stimulating L5b circuits. Our data strongly suggest that L3 harbors the circuitry supporting the generation of up states and that these propagate unidirectionally to deeper layers.

L5b but Not L5a Pyramidal Cells Participate during Up-Down States in the MEC

L5 MEC can be subdivided into two sublayers, 5a (L5a) and 5b (L5b). L5a comprises *etv1*⁺ excitatory cells and projects mostly to the cortex (Kitamura et al., 2017), whereas L5b contains *ctip2*⁺ cells and receives input from the hippocampus (Sürmeli et al., 2015). To compare up state propagation between these two sublayers, we recorded either a L5a or a L5b pyramidal cell simultaneously with a L3 pyramidal cell during spontaneous

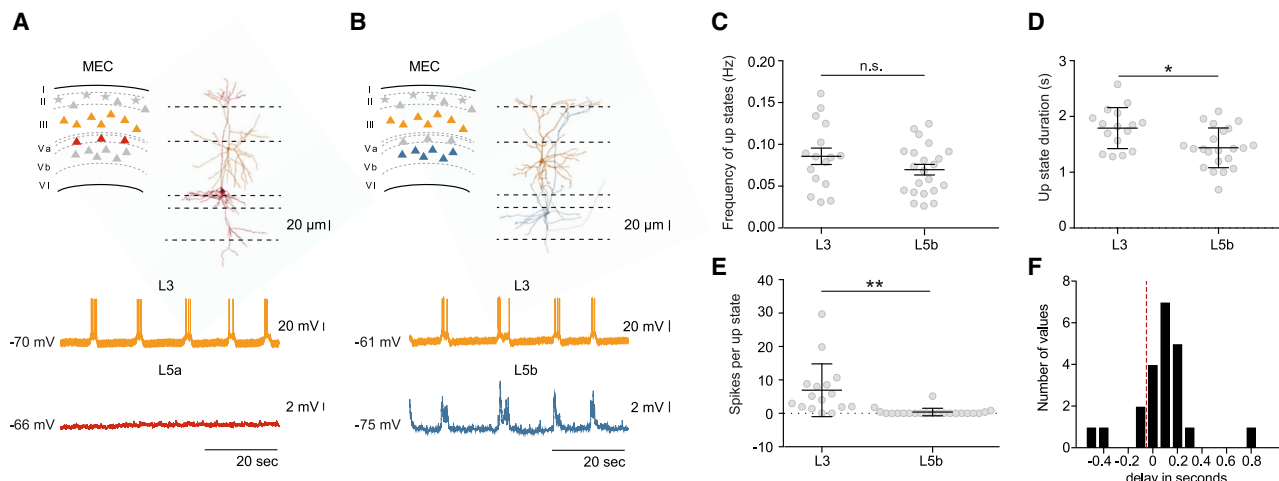


Figure 5. Differential Participation of L5 Pyramidal Cells during UDS

(A) Schematic of the experimental setup. Right panel: reconstruction of biocytin-filled cells with L3 pyramidal cell in orange and L5a pyramidal cell in red. Lower panel: upper trace from L3 pyramidal cell shows clear UDS, and lower trace from L5a pyramidal cell shows the absence of UDS activity.

(B) Schematic of the experimental setup. Right panel: reconstruction of biocytin-filled cells with L3 pyramidal cell in orange and L5b pyramidal cell in blue. Lower panel: upper trace from L3 pyramidal cell shows clear UDS, and lower trace from L5b cells shows synchronous UDS activity.

(C) Frequency of up states were not significantly different between L3 pyramidal cell ($n = 16$ cells) and L5b pyramidal cell ($n = 22$ cells). Most of the L5b pyramidal cells show synchronous UDS with L3 pyramidal cells, as shown in the trace in Figure 4B.

(D) Up state duration was shorter in L5b pyramidal cells ($n = 22$ cells) compared to L3 pyramidal cells ($n = 16$ cells).

(E) L5b pyramidal cells ($n = 22$ cells) mostly showed subthreshold depolarizations during up states with little or no spiking activity, unlike L3 pyramidal cells ($n = 16$ cells).

(F) L5b pyramidal cells followed L3 pyramidal cells as the onset of up states in L5b pyramidal cells experienced a delay when compared to L3 pyramidal cells. Data are presented as means \pm SEMs. n.s. (non significant) for $p > 0.05$, * $p < 0.05$ and ** $p < 0.01$.

UDS (Figures 5A and 5B). To our surprise, of all the duplet recordings from L3 and L5a pyramidal cells, none of the L5a pyramidal cells showed UDS activity, whereas all L5b pyramidal cells had UDS activity that was synchronous with L3 pyramidal cells (Figures 5A and 5B, lower panels). The frequency of up states was the same in the paired L3 and L5b recordings ($L3 = 0.0858 \pm 0.009$ Hz, $n = 16$ cells; $L5b = 0.0714 \pm 0.006$ Hz, $n = 22$ cells; $p = 0.2875$, Mann-Whitney U test; Figure 5C), the duration of up states was shorter in L5b pyramidal cells compared to that of their paired L3 pyramidal cells ($L3 = 1.79 \pm 0.09$ s, $n = 16$ cells; $L5b = 1.44 \pm 0.08$ s, $n = 22$ cells; $p = 0.016$, Mann-Whitney U test; Figure 5D). Furthermore, unlike L3 pyramidal cells, L5b pyramidal cells hardly spiked on up states at resting membrane potential ($L3 = 6.92 \pm 1.98$, $n = 16$ cells; $L5b = 0.39 \pm 0.24$, $n = 22$ cells; $p < 0.0001$, Mann-Whitney U test; Figure 5E). We analyzed the temporal relationship between L3 and L5b pyramidal cells and found that most pyramidal cells in L5b followed the paired L3 pyramidal cell (with a delay of ~ 100 ms; Figure 5F), thereby confirming that in MEC, UDS activity propagates from L3 to L5b.

To conclude, we asked whether the absence of up state propagation to L5a pyramidal cells was due to a lack of synaptic connectivity between L3 and L5a pyramidal cells. We mapped L3 pyramidal cell inputs onto both L5a and L5b pyramidal cells using the *Oxr1* x Chr mice and observed that L5a receive no monosynaptic inputs from L3 pyramidal cells (Figure S5). On the contrary, L5b pyramidal cells received strong and monosynaptic inputs from L3 pyramidal cells, thereby showing synchronized activity during UDS with L3 pyramidal cells.

DISCUSSION

During NREM sleep, the cortex enters a synchronous state characterized by rhythmic UDS. As was previously shown both *in vivo* (Hahn et al., 2012; Isomura et al., 2006) and *in vitro* (Mann et al., 2009; Tahvildari et al., 2012), we demonstrate here that the MEC exhibits prominent UDS activity. Since the MEC is laminated in distinct layers that are associated with different input-output projections, connectivity patterns, and cell types, a laminar profile of UDS activity could shed light on the generation and propagation of such activity. Our results indicate that L3 MEC is the site of origin for UDS in the MEC and that they propagate from there unidirectionally to deeper layers.

Previous work on UDS in the MEC focused on the participation of different neurons in the superficial layers, including excitatory (L3 and L2 cells) and inhibitory neurons (mainly L3; Tahvildari et al., 2012). It was shown that L3 pyramidal cells are most excitable compared to other cell types, and that parvalbumin interneurons are the most strongly modulated among the inhibitory neuron population during UDS in the MEC (Salkoff et al., 2015). It has also been shown that GABAergic transmission is important for the frequency of spikes during up states and in regulating the duration of up states (Mann et al., 2009). We extend these findings by using multi-patch recordings combined with optogenetics in a mouse line (*Oxr1*-Cre) that allows target specificity for L3 MEC, and show that L3 pyramidal cells in the MEC are the generators of UDS in the MEC. We analyzed and compared the spiking activity of L3 pyramidal cells to that of L2 and L5

excitatory neurons at the single-cell level and found that L3 had the most active cell population during UDS in the MEC. In addition, mini-slices of MEC exhibited UDS activity, thereby confirming that MEC alone contains the circuitry that is necessary to generate this slow-wave oscillatory activity.

The L3 MEC occupies an important position both structurally and functionally when considering cortico-hippocampal interactions. Our lab has previously shown that L3 is strongly connected to L2 stellate cells (Winterer et al., 2017). The findings of this study, and the availability of the L3 MEC-specific Cre mouse line, could prompt further investigation, addressing questions as to the role of L3 pyramidal cells during sleep, spatial memory, and behavior. The role of L3 pyramidal cells in development could also be explored. Of note, Namiki and colleagues (2013) studied L3 pyramidal cells in the lateral entorhinal cortex and detected synchronized waves between postnatal days 1 and 6. However, this activity may represent early network oscillations and may thus be different from UDS-related synchrony.

Our findings show that the two L5 sublayers (L5a and L5b) participate differentially during ongoing UDS activity. L5a sends output to distant cortical areas, including the prefrontal cortex (Kitamura et al., 2017; Sürmeli et al., 2015), nucleus accumbens, and amygdala, whereas L5b receives input from the hippocampus as well as from stellate cells in the MEC (Roy et al., 2017; Sürmeli et al., 2015). We report that L5a pyramidal cells do not participate in UDS activity in the MEC and receive no input from L3 pyramidal cells, whereas the activity of L5b is strongly synchronized and follows that of L3 pyramidal cells. This difference could be due to direct synaptic connections between L3 and L5b cells and a lack thereof between L3 and L5a cells (Figure S5). L5b has been shown to receive hippocampal output from both the subiculum and CA1 areas (Ohara et al., 2018), and therefore could be important for the cortical consolidation of hippocampal information by acting as a coincidence detector. As UDS occur *in vivo* during slow-wave NREM sleep, L5b forms an important structural and functional interface between hippocampal sharp wave activity and cortical UDS activity.

In conclusion, our finding that L3 orchestrates UDS within the MEC is an important piece of the puzzle for understanding entorhinal-hippocampal information flow. Up-down state transitions in superficial layers have been shown to propagate to the hippocampus (Sirota et al., 2003) and facilitate hippocampal sharp waves (Sirota et al., 2003; Isomura et al., 2006; Mölle et al., 2006). Conversely, sharp waves in CA1 precede sharp wave-like LFP patterns in the deep layers of the entorhinal cortex (Chrobak and Buzsáki, 1996). Thus, the local spread of UDS from L3 to L5b reported here may activate the hippocampus to replay stored patterns and at the same time set the L5b pyramidal cells in a “receive mode” to read out the hippocampal output in the form of integration or coincidence detection. Considering the findings presented here, one can envisage future studies to further dissect the role of different cortico-hippocampal pathways during slow-wave sleep and behavior.

STAR★METHODS

Detailed methods are provided in the online version of this paper and include the following:

- KEY RESOURCES TABLE
- RESOURCE AVAILABILITY
 - Lead Contact
 - Materials Availability
 - Data and Code Availability
- EXPERIMENTAL MODEL AND SUBJECT DETAILS
- METHOD DETAILS
 - Surgery
 - *In Vivo* Recordings
 - Analysis of *In Vivo* Data
 - *In Vitro* Slice Preparation
 - *In Vitro* Electrophysiology
 - Calcium Imaging
 - Histological Procedure
 - Analysis of *In Vitro* Data
- QUANTIFICATION AND STATISTICAL ANALYSES

SUPPLEMENTAL INFORMATION

Supplemental Information can be found online at <https://doi.org/10.1016/j.celrep.2020.108470>.

ACKNOWLEDGMENTS

We would like to thank Susanne Rieckmann and Anke Schönherr for excellent technical assistance. This work was supported by the Stiftung Charité, to P.B., H.M., and A.C.; the NeuroCure Cluster of Excellence; the DZNE; the Einstein Foundation; and the Deutsche Forschungsgemeinschaft (to D.S. [DFG Project number 327654276—SFB 1315, SFB 958, and Exc 257] and F.W.J. [JO1079/1-1; JO1079/3-1; and SFB665]).

AUTHOR CONTRIBUTIONS

P.B., C.H., F.W.J., A.C., H.M., and D.S. designed the experiments; P.B., R.d.F., C.H., and A.C. performed the research; P.B., R.d.F., C.H., F.W.J., and C.L. analyzed the data; P.B. wrote the paper with the help of R.d.F., C.H., F.W.J., A.C., H.M., and D.S. All of the authors read and edited the final version of the manuscript.

DECLARATION OF INTERESTS

The authors declare no competing interests.

Received: June 20, 2018

Revised: June 26, 2020

Accepted: November 10, 2020

Published: December 8, 2020

REFERENCES

- Bartram, J., Kahn, M.C., Tuohy, S., Paulsen, O., Wilson, T., and Mann, E.O. (2017). Cortical up states induce the selective weakening of subthreshold synaptic inputs. *Nat. Commun.* 8, 665.
- Chrobak, J.J., and Buzsáki, G. (1996). High-frequency oscillations in the output networks of the hippocampal-entorhinal axis of the freely behaving rat. *J. Neurosci.* 16, 3056–3066.
- Craig, M.T., Mayne, E.W., Bettler, B., Paulsen, O., and McBain, C.J. (2013). Distinct roles of GABAB1a- and GABAB1b-containing GABAB receptors in spontaneous and evoked termination of persistent cortical activity. *J. Physiol.* 591, 835–843.
- Fuchs, E.C., Neitz, A., Pinna, R., Melzer, S., Caputi, A., and Monyer, H. (2016). Local and Distant Input Controlling Excitation in Layer II of the Medial Entorhinal Cortex. *Neuron* 89, 194–208.

- Gardner, R.J., Lu, L., Wernle, T., Moser, M.B., and Moser, E.I. (2019). Correlation structure of grid cells is preserved during sleep. *Nat. Neurosci.* 22, 598–608.
- Goebbels, S., Bormuth, I., Bode, U., Hermanson, O., Schwab, M.H., and Nave, K.A. (2006). Genetic targeting of principal neurons in neocortex and hippocampus of NEX-Cre mice. *Genesis* 44, 611–621.
- González-Rueda, A., Pedrosa, V., Feord, R.C., Clopath, C., and Paulsen, O. (2018). Activity-Dependent Downscaling of Subthreshold Synaptic Inputs during Slow-Wave-Sleep-like Activity In Vivo. *Neuron* 97, 1244–1252.e5.
- Hahn, T.T., McFarland, J.M., Berberich, S., Sakmann, B., and Mehta, M.R. (2012). Spontaneous persistent activity in entorhinal cortex modulates cortico-hippocampal interaction in vivo. *Nat. Neurosci.* 15, 1531–1538.
- Isomura, Y., Sirota, A., Ozen, S., Montgomery, S., Mizuseki, K., Henze, D.A., and Buzsáki, G. (2006). Integration and segregation of activity in entorhinal-hippocampal subregions by neocortical slow oscillations. *Neuron* 52, 871–882.
- Kitamura, T., Pignatelli, M., Suh, J., Kohara, K., Yoshiki, A., Abe, K., and Tonegawa, S. (2014). Island cells control temporal association memory. *Science* 343, 896–901.
- Kitamura, T., Ogawa, S.K., Roy, D.S., Okuyama, T., Morrissey, M.D., Smith, L.M., Redondo, R.L., and Tonegawa, S. (2017). Engrams and circuits crucial for systems consolidation of a memory. *Science* 356, 73–78.
- Luczak, A., Barthó, P., Marguet, S.L., Buzsáki, G., and Harris, K.D. (2007). Sequential structure of neocortical spontaneous activity in vivo. *Proc. Natl. Acad. Sci. USA* 104, 347–352.
- Madisen, L., Garner, A.R., Shimaoka, D., Chuong, A.S., Klapoetke, N.C., Li, L., van der Bourg, A., Niino, Y., Egolf, L., Monetti, C., et al. (2015). Transgenic mice for intersectional targeting of neural sensors and effectors with high specificity and performance. *Neuron* 85, 942–958.
- Mann, E.O., Kohl, M.M., and Paulsen, O. (2009). Distinct roles of GABA(A) and GABA(B) receptors in balancing and terminating persistent cortical activity. *J. Neurosci.* 29, 7513–7518.
- Massimini, M., Huber, R., Ferrarelli, F., Hill, S., and Tononi, G. (2004). The sleep slow oscillation as a traveling wave. *J. Neurosci.* 24, 6862–6870.
- Mölle, M., Yeshenko, O., Marshall, L., Sara, S.J., and Born, J. (2006). Hippocampal sharp wave-ripples linked to slow oscillations in rat slow-wave sleep. *J. Neurophysiol.* 96, 62–70.
- Namiki, S., Norimoto, H., Kobayashi, C., Nakatani, K., Matsuki, N., and Ikegaya, Y. (2013). Layer III neurons control synchronized waves in the immature cerebral cortex. *J. Neurosci.* 33, 987–1001.
- Neske, G.T. (2016). The Slow Oscillation in Cortical and Thalamic Networks: Mechanisms and Functions. *Front. Neural Circuits* 9, 88.
- Neske, G.T., Patrick, S.L., and Connors, B.W. (2015). Contributions of diverse excitatory and inhibitory neurons to recurrent network activity in cerebral cortex. *J. Neurosci.* 35, 1089–1105.
- Nir, Y., Staba, R.J., Andrillon, T., Vyazovskiy, V.V., Cirelli, C., Fried, I., and Tononi, G. (2011). Regional slow waves and spindles in human sleep. *Neuron* 70, 153–169.
- Ohara, S., Onodera, M., Simonsen, Ø.W., Yoshino, R., Hioki, H., Iijima, T., Tsutsui, K.I., and Witter, M.P. (2018). Intrinsic Projections of Layer Vb Neurons to Layers Va, III, and II in the Lateral and Medial Entorhinal Cortex of the Rat. *Cell Rep.* 24, 107–116.
- Pachitariu, M., Steinmetz, N., Kadir, S., Carandini, M., and Harris, K.D. (2016). Fast and accurate spike sorting of high-channel count probes with KiloSort. In *Advances in Neural Information Processing Systems* 29, D.D. Lee, M. Sugiyama, U.V. Luxburg, I. Guyon, and R. Garnett, eds., <https://discovery.ucl.ac.uk/id/eprint/1557035>.
- Roy, D.S., Kitamura, T., Okuyama, T., Ogawa, S.K., Sun, C., Obata, Y., Yoshiki, A., and Tonegawa, S. (2017). Distinct Neural Circuits for the Formation and Retrieval of Episodic Memories. *Cell* 170, 1000–1012.e19.
- Rueckl, M., Lenzi, S.C., Moreno-Velasquez, L., Parthier, D., Schmitz, D., Ruegger, S., and Jochenning, F.W. (2017). SamuROI, a Python-Based Software Tool for Visualization and Analysis of Dynamic Time Series Imaging at Multiple Spatial Scales. *Front. Neuroinform.* 11, 44.
- Salkoff, D.B., Zagha, E., Yüzgeç, Ö., and McCormick, D.A. (2015). Synaptic Mechanisms of Tight Spike Synchrony at Gamma Frequency in Cerebral Cortex. *J. Neurosci.* 35, 10236–10251.
- Sanchez-Vives, M.V., and McCormick, D.A. (2000). Cellular and network mechanisms of rhythmic recurrent activity in neocortex. *Nat. Neurosci.* 3, 1027–1034.
- Schindelin, J., Arganda-Carreras, I., Frise, E., Kaynig, V., Longair, M., Pietzsch, T., Preibisch, S., Rueden, C., Saalfeld, S., Schmid, B., et al. (2012). Fiji: an open-source platform for biological-image analysis. *Nat. Methods* 9, 676–682.
- Schneider, C.A., Rasband, W.S., and Eliceiri, K.W. (2012). NIH Image to ImageJ: 25 years of image analysis. *Nat. Methods* 9, 671–675.
- Seamari, Y., Narváez, J.A., Vico, F.J., Lobo, D., and Sanchez-Vives, M.V. (2007). Robust off- and online separation of intracellularly recorded up and down cortical states. *PLOS ONE* 2, e888.
- Sirota, A., Csicsvari, J., Buhl, D., and Buzsáki, G. (2003). Communication between neocortex and hippocampus during sleep in rodents. *Proc. Natl. Acad. Sci. USA* 100, 2065–2069.
- Steriade, M., Nuñez, A., and Amzica, F. (1993). A novel slow (< 1 Hz) oscillation of neocortical neurons in vivo: depolarizing and hyperpolarizing components. *J. Neurosci.* 13, 3252–3265.
- Stockwell, R.G., Mansinha, L., and Lowe, R.P. (1996). Localization of the complex spectrum: the S transform. *IEEE Trans. Signal Process.* 44, 998–1001.
- Suh, J., Rivest, A.J., Nakashiba, T., Tominaga, T., and Tonegawa, S. (2011). Entorhinal cortex layer III input to the hippocampus is crucial for temporal association memory. *Science* 334, 1415–1420.
- Sürmeli, G., Marcu, D.C., McClure, C., Garden, D.L.F., Pastoll, H., and Nolan, M.F. (2015). Molecularly Defined Circuitry Reveals Input-Output Segregation in Deep Layers of the Medial Entorhinal Cortex. *Neuron* 88, 1040–1053.
- Tahvildari, B., Wölfel, M., Duque, A., and McCormick, D.A. (2012). Selective functional interactions between excitatory and inhibitory cortical neurons and differential contribution to persistent activity of the slow oscillation. *J. Neurosci.* 32, 12165–12179.
- Trettel, S.G., Trimmer, J.B., Hwaun, E., Fiete, I.R., and Colgin, L.L. (2019). Grid cell co-activity patterns during sleep reflect spatial overlap of grid fields during active behaviors. *Nat. Neurosci.* 22, 609–617.
- Tukker, J.J., Beed, P., Schmitz, D., Larkum, M.E., and Sachdev, R.N.S. (2020). Up and Down States and Memory Consolidation Across Somatosensory, Entorhinal, and Hippocampal Cortices. *Front. Syst. Neurosci.* 14, 22.
- Vyazovskiy, V.V., Olcese, U., Hanlon, E.C., Nir, Y., Cirelli, C., and Tononi, G. (2011). Local sleep in awake rats. *Nature* 472, 443–447.
- Wilson, C.J., and Groves, P.M. (1981). Spontaneous firing patterns of identified spiny neurons in the rat neostriatum. *Brain Res.* 220, 67–80.
- Winterer, J., Maier, N., Wozny, C., Beed, P., Breustedt, J., Evangelista, R., Peng, Y., D'Albis, T., Kempter, R., and Schmitz, D. (2017). Excitatory Microcircuits within Superficial Layers of the Medial Entorhinal Cortex. *Cell Rep.* 19, 1110–1116.

STAR★METHODS

KEY RESOURCES TABLE

REAGENT or RESOURCE	SOURCE	IDENTIFIER
Antibodies		
Streptavidin Alexa 488 Conjugate	Invitrogen	Cat# S32354; RRID: AB_2315383
Streptavidin Alexa 555 Conjugate	Invitrogen	Cat# s21381; RRID: AB_2307336
Rat monoclonal anti-CTIP2	Abcam	Cat# ab18465; RRID: AB_2064130
Rabbit monoclonal anti-WFS1	Proteintech	Cat# 11558-1-AP; RRID: AB_2216046
Chicken monoclonal anti-GFP	Abcam	Cat# ab92456; RRID: AB_10561923
Guinea pig monoclonal anti-NeuN	Merck	Cat# ABN90
Goat anti-rat Alexa 555 Conjugate	Invitrogen	Cat# A-21434; RRID: AB_141733
Goat anti-guinea pig Alexa 405 conjugate	Abcam	Abcam Cat# ab175678; RRID: AB_2827755
Bacterial and Virus Strains		
pAAV-Ef1a-DIO eNpHR 3.0-EYFP	Gift from Karl Deisseroth	Deisseroth stock
Chemicals, Peptides, and Recombinant Proteins		
Urethane	Sigma Aldrich	Cat #U2500
Dil	ThermoFisher	Cat #D3911
RuBi-GABA	Tocris	Cat #3400
Deposited Data		
Raw and analyzed data	This paper	https://doi.org/10.6084/m9.figshare.13154321.v1 and upon author request
Experimental Models: Organisms/Strains		
Mouse: C57Bl6/n	Charité Forschungseinrichtung für Experimentelle Medizin	N/A
Nex-Cre mice	Charité Forschungseinrichtung für Experimentelle Medizin	RRID:MGI:3835559
Mouse: Ai95(RCL-GCaMP6f)-D	The Jackson Laboratory	JAX stock #024105
Mouse: C57BL/6N-Tg(Oxr1-cre)C14Stl/J	The Jackson Laboratory	JAX stock #030484
Mouse: Ai40(RCL-ArchT/EGFP)-D	The Jackson Laboratory	JAX stock #021188
Mouse: Ai32(RCL-ChR2(H134R)/EYFP)	The Jackson Laboratory	JAX stock # 012569
Mouse: STOCK Tg(Uchl1-cre)NO63Gsat/Mmucd	Mutant Mouse Resource and & Research Centers	RRID:MMRRC_036089-UCD
Software and Algorithms		
Fiji	Schindelin et al., 2012	https://fiji.sc/wiki/index.php/Fiji
ImageJ	Schneider et al., 2012	https://imagej.nih.gov/ij/
MATLAB 2019b	MathWorks	https://de.mathworks.com/?s_tid=gn_logo
Simulink	Mathworks	https://de.mathworks.com/products/simulink.html
Axon pClamp10 10.6.2	Molecular Devices	https://mdc.custhelp.com/app/answers/detail/a_id/18779/~/axon%E2%84%A2pclamp%E2%84%A2-10-electrophysiology-data-acquisition-%26-analysis-software-download
iQ live cell imaging software	Andor	https://andor.oxinst.com/products/iq-live-cell-imaging-software/
MAUDs Algorithm	Seamari et al., 2007	http://www.geb.uma.es/mauds
Kilosort2 (Pachitariu et al., 2016)	Pachitariu et al., 2016	https://github.com/MouseLand/Kilosort
Prism	GraphPad	https://www.graphpad.com/scientific-software/prism/
SAMUROI python package	Rueckl et al., 2017	https://github.com/samuroi/SamuROI
Code related to this paper	This paper	https://github.com/Schmitz-lab/MEC-Up-States and upon author request

(Continued on next page)

Continued

REAGENT or RESOURCE	SOURCE	IDENTIFIER
Other		
Neurostar Robot Stereotax	NeuroStar	https://robot-stereotaxic.com/drill-injection-robot/
Silicon probes and optrodes	NeuroNexus	https://neuronexus.com/wp-content/uploads/2018/11/2019_NNxCatalog_20181113.pdf
RHD2000 recording system	Intan	http://intantech.com/RHD_system.html
525nm PlexBright LED	Plexon	https://plexon.com/products/plexbright-table-top-modules/#1501022507108-0524a9b7-10bf
BNC-2110 Shielded Connector Block	National Instruments	Cat # 777643-01
DMI4000 B Fluorescence Microscope	Leica	https://www.leica-microsystems.com/products/light-microscopes/p/leica-dmi4000-b/
Vt1200 Semiautomatic vibrating blade microtome	Leica	https://www.leicabiosystems.com/histology-equipment/sliding-and-vibrating-blade-microtomes/vibrating-blade-microtomes/leica-vt1200/
BX61WI Upright microscope	Olympus	https://www.olympus-lifescience.com/en/microscopes/upright/bx61wi/
DMZ Universal Puller	Zeitz	https://www.zeitz-puller.com/
Multiclamp 700A/B Amplifiers	Science Products	https://science-products.com/en/shop/23/9/amplifiers-etc/amplifiers/patchclamp_amplifier/axon-multiclamp-700b
Axon Digidata 1550B data acquisition system	Molecular Devices	https://www.moleculardevices.com/products/axon-patch-clamp-system/digitizers/axon-digidata-1550b-plus-humsilencer#ref
Borosilicate glass capillaries	Harvard Apparatus	Cat# W330-0057
CoolLED pE-300	CoolLED	https://www.cooled.com/
ISO-Flex Stimulus Isolator	A.M.P.I.	http://www.ampi.co.il/isoflex.html
CSU22 Spinning Disk Microscope	Yokogawa	https://www.yokogawa.com/de/solutions/discontinued/csu22/
488nm Laser	Coherent	https://www.coherent.com/lasers/main/sapphire-lasers
Ixon DU-897D CCD	Andor	http://ocult.mit.edu/instrumentation/MORIS/Documents/DU-897_BI.pdf

RESOURCE AVAILABILITY

Lead Contact

Further information and requests related to this study should be directed to and will be fulfilled by the lead contact, Prateep Beed (prateep.beed@charite.de).

Materials Availability

This study did not generate new unique reagents.

Data and Code Availability

The datasets and code supporting related to this study can be found on online repositories (see [Key Resources Table](#)), or upon request to the lead author. Original data have been deposited to Figshare: <https://doi.org/10.6084/m9.figshare.13154321.v1>.

EXPERIMENTAL MODEL AND SUBJECT DETAILS

All *in vivo* experiments were conducted according to regulations of the Berlin Landesamt für Gesundheit und Soziales (G0150/17). All animal maintenance for *in vitro* experiments was performed in accordance with Berlin Landesamt für Gesundheit und Soziales (Berlin T 0100/03).

For the first portion of this study (Figure 1), adult C57Bl6/n mice of both sexes were used. For subsequent experiments, L3-specific Oxr1-Cre mice (<https://www.jax.org/strain/030484>, Suh et al., 2011) were crossed with Ai40D mice (<https://www.jax.org/strain/021188>) or Ai32 mice (<https://www.jax.org/strain/012569>, Madisen et al., 2015) for selective expression of archaeorhodopsin or

channelrhodopsin, respectively. Uchl1-Cre mice were obtained from the Mutant Mouse Regional Resource Center. (MMRC, USA, Fuchs et al., 2016). For calcium imaging experiments, Nex-Cre mice (Goebbels et al., 2006) were crossed with Ai95 animals (<https://www.jax.org/strain/024105>; Madisen et al., 2015) for constitutive GCaMP6f expression in pyramidal cells only. Naive offspring of both sexes for all lines were used. Analyses of the influence of sex in our results were not performed due to small sample sizes. Adult mice ($p > 30$) were used for *in vivo* experiments (Figures 3 and S4), whereas brain slices for *in vitro* experiments were obtained from mice p12–18 (Figures 1, 2, 4, 5, S1, S2, and S3) and p12–28 (Figures 3 and S5). All animals were housed with a 12-hour light/dark cycle in group cages, with *ad libitum* access to water and standard rodent chow.

METHOD DETAILS

Surgery

For viral injections, mice were deeply anaesthetized with 2% isoflurane and a craniotomy was performed, exposing the transverse sinus 3.3ML from the midline. An injection needle was slowly lowered 0.3mm anterior to the edge of the sinus at an angle of -8° in the antero-posterior axis to a depth of 1.8DV using a micromanipulator. 500nl of pAAV-Ef1a-DIO eNpHR 3.0-EYFP (a gift from Karl Deisseroth; Addgene viral prep # 26966-AAV1) was injected at a speed of 50nl/min (Neurostar, Tübingen, Germany), waiting several minutes before withdrawing the needle. Mice were provided with carprofen and metamizol and left to recover for one month in their home cages before acute recordings.

For acute recordings, mice were deeply anaesthetized by intraperitoneal injection of a 10% urethane solution (1–1.5g/kg, Sigma Aldrich, Munich Germany). A craniotomy was performed above the MEC based on coordinates from the Paxinos and Franklin Brain Atlas (2001) at approximately ± 3.3 ML and 0.5 anterior to lambda.

32-channel linear silicone probes or optrodes (NeuroNexus, Ann Arbor MI) were painted with the fluorescent dye Dil (Thermo Fisher Scientific, Schwerte Germany) and lowered slowly into the craniotomy at a 20° angle in the sagittal plane using a micromanipulator. An Ag/AgCl ground wire was placed into a well with saline anterior to the recording site. Signals were sampled at 20KHz with an RHD2000 amplifier (Intan Technologies, Los Angeles, California), and visualized using on-board recording software. Recordings began after a minimum 10 min waiting period at a depth at which clear up states could consistently be seen at a frequency of approximately 0.1Hz. During recordings, body temperature was maintained at 36° using a heating pad.

In Vivo Recordings

For optogenetic pulse barrage experiments, a 10 min baseline was first recorded. Then, a 10Hz light ON protocol (for 5 s) was applied using a 525nm PlexBright LED (Plexon, Dallas TX) coupled directly to the silicon optrode. This was repeated after a 5 s light OFF period. These dual barrages were repeated every 10 s over 20 min.

A closed-loop optogenetic stimulation system was created by routing one channel of the LFP via a National Instruments BNC-2110 shielded connector block (National Instruments, Austin TX) to a computer running Simulink (Mathworks, Natick NJ). Whenever a threshold detecting event was detected, a pulse was emitted to the LED, with a delay of approximately 50ms (data not shown).

After recordings were completed, mice were given a further urethane overdose, then perfused transcardially with 0.1M PBS followed by 4% paraformaldehyde. Brains were kept in PFA overnight, then sliced using a vibratome (Leica Microsystems, Wetzlar Germany) into $100\mu\text{M}$ sagittal slices and mounted for post hoc anatomical identification of recording sites and immunohistochemical stainings (see ‘[Histological Procedure](#)’, below). Images of probe tracks and stainings were obtained using a Leica DMI 4000B fluorescence microscope (Leica, Wetzlar, Germany). Only recordings with clear probe tracks in superficial layers of the MEC were used for subsequent analysis.

Analysis of In Vivo Data

All analysis was performed using custom scripts written in MATLAB (Mathworks, Natick NJ). For each recording, a sample channel was taken from the tip of the silicon probe in L3, and down-sampled from 20 to 0.2 kHz. Up states were detected using a modified version of the MAUDs algorithm (Seamari et al., 2007). Briefly, the LFP was filtered between 1 and 4 Hz, and smoothed using a Savitzky-Golay filter. Deflections two standard deviations above the median were calculated with a moving window, and compared with periods of elevated multiunit activity extracted with Kilosort2 (Pachitariu et al., 2016) to find indices of up states. From these indices, the spectral content of these up states could be calculated with the Stockwell Transform (Stockwell et al., 1996), as well as information about their duration and frequency.

The effect of LED pulse barrages was calculated by detecting the number of up states occurring inside of stimulation epochs, and comparing it to the same number of light OFF epochs of equivalent length (i.e., 50ms) randomly sampled from the rest of the recording.

The effect of closed loop stimulation was measured by comparing the properties of up states detected in a 10 min baseline and 10 min period of stimulation.

In vitro Slice Preparation

Near horizontal slices ($\sim 15^\circ$ off the horizontal plane) of the medial entorhinal cortex (MEC) were obtained from C57Bl6/n mice. Animals were anesthetized with isoflurane and decapitated. The brains were quickly removed and placed in ice-cold ($\sim 4^\circ\text{C}$) artificial cerebrospinal fluid (ACSF) (pH 7.4) containing (in mM) 85 NaCl, 25 NaHCO₃, 75 Sucrose, 10 Glucose, 2.5 KCl, 1.25 NaH₂PO₄,

3.5MgSO₄, 0.5 CaCl₂, and aerated with 95% O₂, 5% CO₂. Tissue blocks containing the brain region of interest were mounted on a vibratome (Leica VT 1200, Leica Microsystems), cut at 400 μm thickness, and incubated at 35°C for 30 min. In the case of mini-slices a needle (diameter = 0.60 mm) was used to dissect the MEC from the LEC and the hippocampus proper. The slices were then transferred to ACSF containing (in mM) 85 NaCl, 25 NaHCO₃, 75 Sucrose, 10 Glucose, 2.5 KCl, 1.25 NaH₂PO₄, 3.5 MgSO₄, 0.5 CaCl₂. The slices were stored at room temperature in a submerged chamber for 1–5 hr before being transferred to the recording chamber.

In Vitro Electrophysiology

For recordings, a slice was transferred to a submersion style recording chamber located on the stage of an upright, fixed-stage microscope (BX51WI, Olympus, Hamburg Germany) equipped with a water immersion objective and a near-infrared charge-coupled device (CCD) camera. The slices were perfused with ACSF (~35°C bubbled with 95% O₂–5% CO₂) at 3–5 ml/min to maintain neuronal health throughout the slice. The ACSF had the same composition as the incubation solution except for the concentrations of calcium and magnesium, which were reduced to 1.2 and 1.0 mM, respectively. Recording electrodes with impedance of 3–5 MΩ were pulled from borosilicate glass capillaries (Harvard Apparatus, Kent, UK; 1.5 mm OD) using a micropipette electrode puller (DMZ Universal Puller, Zeitz, Martinsried Germany). The intracellular solution contained the following (in mM): 135 K-glucuronate, 6 KCl, 2 MgCl₂, 0.2 EGTA, 5 Na₂-phosphocreatine, 2 Na₂-ATP, 0.5 Na₂-GTP, 10 HEPES buffer, and 0.2% biocytin. The pH was adjusted to 7.2 with KOH. Recordings were performed using Multiclamp 700A/B amplifiers (Science Products, Hofheim Germany). The seal resistance was >1 GΩ. Capacitance compensation was maximal and bridge balance adjusted. Signals were filtered at 6 kHz, sampled at 20 kHz, and digitized using the Digidata 1550 and pClamp 10 (Molecular Devices, San Jose, CA, USA).

Stimulation experiments were performed using a bipolar micro-electrode (glass pipet filled with ACSF solution, wrapped by a fine grounding wire). A 4x objective was used to visually guide the stimulating electrode into the MEC. The inter-stimulus interval was ten seconds with a duration of 50 μs for each stimulus, using an isolated voltage stimulator (ISO-Flex, A.M.P.I., Israel).

In vitro GABA uncaging was done by a blue light LED (CoolLED pE-300 system with 470nm light) which photolysed the caged Rubi-GABA (Tocris, UK). When a spike was detected on an upstate, 500ms of blue light was used to uncage Rubi-GABA. *In vitro* optogenetic stimulation was done using a green light LED for stimulation of ArchT positive cells. For current and voltage clamp recordings of ArchT mediated hyperpolarization we used a 500ms light pulse. For suppression of spikes we used 50ms light pulse at 19Hz for 2 s.

Calcium Imaging

For population Ca²⁺ imaging of neonatal spontaneous synchronous network events, the genetically encoded Ca²⁺ indicator (GECI) GCaMP6f was used. Ca²⁺ imaging was performed using a Yokogawa CSU-22 spinning disc microscope (Yokogawa, Wehr, Germany) at 5000rpm. The spinning disc confocal permitted the generation of a large field of view time series at a high acquisition rate. A 488nm laser (Coherent, Santa Clara, CA, USA) was focused onto the field of view using a 4x, 40x or 60x objective. Emission light was filtered using a 515 ± 15nm bandpass filter. Fluorescence was detected using an Andor Ixon DU-897D back-illuminated CCD (Andor, Belfast, UK), with a pixel size of 16μm. Andor iQ software was used for data acquisition.

For data analysis, we used the SAMUROI python package (Rueckl et al., 2017) in combination with custom python routines. Events were detected using a template matching based algorithm, the onset was determined as the time point in an event when the signal reached two standard deviations above the mean standard deviation of the baseline. Signal onsets were used for synchrony analysis.

Histological Procedure

At the end of the recording session, the electrode was carefully detached from the recorded cell and the slice was fixed with 4% paraformaldehyde in 0.1 M phosphate buffer (PB) for at least 24 h at 4°C, then washed three times in 0.1 M PBS. Slices were then incubated in PBS containing 1% Triton X-100 and 5% normal goat serum for 4 hr at room temperature (RT). To visualize biocytin-filled cells we used Streptavidin Alexa 488/ 555 conjugate (S32354/S21381, 1:500, Invitrogen). CTIP2 (1:500 Rat, Abcam, Cambridge, UK) was used to visualize L5b, WFS1 (1:1000, Rabbit, Proteintech, IL, USA) to visualize L2 border with L3 as it stains for L2 pyramids in the MEC, antiGFP (ab18465, 1:1000, Chicken, Abcam, Cambridge, UK) for visualizing the expression of Arch in the Oxr1-Cre x Ai40D mice, and NeuN for visualizing neuronal cell bodies (ABN90, 1:1000, Guinea Pig, Millipore, Darmstadt Germany). Slices were incubated with primary antibodies for 48 hr at RT. After rinsing two times in PBS, sections were incubated in the PBS solution containing 0.5% Triton X-100, and Streptavidin Alexa 488/ 555 conjugate (for biocytin-filled neurons, S32354/ s21381, Invitrogen Corporation, Carlsbad, CA) or goat anti-rat conjugated with Alexa fluor 555 (for CTIP2, A-21434, 1:500 Invitrogen Corporation, Carlsbad, CA) or goat anti-guinea pig Alexa fluor 405 (for NeuN, ab175678, Abcam, Cambridge UK). Slices were mounted in Mowiol (Sigma Aldrich, Darmstadt Germany) under coverslips 2–3 hr after incubation with the secondary antibodies and stored at 4°C. Labeled cells were visualized using 20x or 40x objectives on a confocal microscope system (Leica, Wetzlar Germany). Z stack projections were optimized to examine the full extent of somato-dendritic compartments and axonal arborization. Image stacks obtained were registered and combined in Fiji (Schindelin et al., 2012) to form a montage of the sections.

Analysis of In Vitro Data

Up state onset, frequency and duration *in vitro* were quantified by using a modified version of the MAUDS algorithm that was published in Seamari et al. (2007). Spike probability is defined as the ration of the number of up states with spikes to total number of up states, spike frequency is the total number of spikes divided by the whole recording time and spikes per up state denotes the number

of spikes elicited only during up states. Analyses were performed using custom scripts written in MATLAB (The MathWorks, Natick, MA), Microsoft Office Excel (Microsoft, Redmond, WA), and ImageJ ([Schneider et al., 2012](#)).

QUANTIFICATION AND STATISTICAL ANALYSES

No randomization or blinding was performed during the execution of experiments or data analysis for this paper. No statistical methods were used for predetermining sample sizes. Data are presented in figures as mean \pm SEM unless otherwise stated. Statistical analyses were performed using MATLAB (The MathWorks, Natick, MA), and Graphpad Prism (La Jolla, CA, USA). For data violating assumptions of normality (determined via a Kolmogorov-Smirnov test), non-parametric tests were used. Reported p values were all based on tests mentioned in the text. Significance was accepted at $p < 0.05$ and labeled as: n.s. (non significant) for $p > 0.05$, * $p < 0.05$ and ** $p < 0.01$.